PNAS RESEARCH ARTICLE | NEUROSCIENCE

Loss of $Ca_V1.3$ RNA editing enhances mouse hippocampal plasticity, learning, and memory

Jing Zhai[a], Sheeja Navakkode[a,b], Sean Qing Zhang Yeow[a], Kumar Krishna-K[a], Mui Cheng Liang[a], Joanne Huifen Koh[a], Rui Xiong Wong[a], Wei Ping Yu[c], Sreedharan Sajikumar[a,d], Hua Huang[a,e,1], and Tuck Wah Soong[a,d,1]

Edited by Hee-Sup Shin, Institute for Basic Science, Daejeon, Korea (South); received March 4, 2022; accepted June 20, 2022

L-type $Ca_V1.3$ calcium channels are expressed on the dendrites and soma of neurons, and there is a paucity of information about its role in hippocampal plasticity. Here, by genetic targeting to ablate $Ca_V1.3$ RNA editing, we demonstrate that unedited $Ca_V1.3^{\Delta ECS}$ mice exhibited improved learning and enhanced long-term memory, supporting a functional role of RNA editing in behavior. Significantly, the editing paradox that functional recoding of $Ca_V1.3$ RNA editing sites slows Ca^{2+}-dependent inactivation to increase Ca^{2+} influx but reduces channel open probability to decrease Ca^{2+} influx was resolved. Mechanistically, using hippocampal slice recordings, we provide evidence that unedited $Ca_V1.3$ channels permitted larger Ca^{2+} influx into the hippocampal pyramidal neurons to bolster neuronal excitability, synaptic transmission, late long-term potentiation, and increased dendritic arborization. Of note, RNA editing of the $Ca_V1.3$ IQ-domain was found to be evolutionarily conserved in mammals, which lends support to the importance of the functional recoding of the $Ca_V1.3$ channel in brain function.

RNA editing | $Ca_V1.3$ calcium channel | hippocampal plasticity | spatial learning and memory

Hard-wired genomic mutations can be passed down the generations, but flexible RNA editing, which varies between 0 and 100%, can generate various levels of editing in a developmental and spatiotemporal manner. This posttranscriptional process can correspondingly alter protein function or level through recoding codons or through either affecting alternative splicing or noncoding RNA binding. Adenosine-to-inosine (A-to-I) RNA editing is catalyzed by adenosine deaminases acting on RNA (ADAR) enzymes. In humans, it has been reported that the editome contains millions of editing sites, but they are mostly found in noncoding sites (1, 2). However, there are also multiple substrates in human transcripts coding for ion channels or transporters that are important for brain function (3). Of interest, ~60,000 recoding A-to-I RNA editing sites have been uncovered in the *Drosophila* and in cephalopods, such as squid and octopus (4), but there is a paucity of information on the functional and behavioral importance of RNA editing, especially in mammals. In cephalopods, voltage-gated potassium channel $K_V1.1$ RNA editing is associated with cold adaptation, while causality has not been demonstrated (5).

It has been postulated that most mammalian nonsynonymous recoding RNA editing sites are nonadaptive, but it is still unclear whether the functional editing recoding—that is, the recoding of the genomic codon in the transcript that results in an amino acid and subsequent functional change—has critical physiological significance. However, a counterargument is that conserved high-level recoding RNA editing sites in mammals could be functionally advantageous. The ablation of RNA editing of glutamate ionotropic receptor AMPA type subunit 2 (GluA2) resulted in epilepsy and death in a few weeks (6), while the generation of knock-in VGV serotonin 2C receptors ($5\text{-}HT_{2C}$) edited mice showed a loss of fat mass and characteristics of anxiety and depression (7, 8). The dearth of investigations into altered behavior and the functional effects of mammalian RNA editing in cognitive functions led us to investigate whether mice genetically targeted to harbor only unedited $Ca_V1.3$ channels would experience effects on hippocampal learning and memory because the editing level of the first site of the $Ca_V1.3$ IQ-domain *IQDY* (ATA→ATG; *I*→*M*) residue in the mouse hippocampus can reach 50% (9). In addition, such mice allowed us to resolve the $Ca_V1.3$ RNA editing paradox because RNA editing of the $Ca_V1.3$ IQ-domain slows Ca^{2+}-dependent inactivation to allow larger entry of Ca^{2+} ions (9), while in contrast, editing attenuates apo-calmodulin interaction with the IQ domain to decrease channel open probability to reduce Ca^{2+} influx (10, 11).

Here, we show that $Ca_V1.3$ RNA editing is evolutionarily conserved and the editing level is down-regulated during learning. Loss of $Ca_V1.3$ IQ-domain RNA editing is a gain of function to admit larger Ca^{2+} influx, and thus the result obtained in neurons resolves the editing paradox. The neurophysiological consequence of a larger Ca^{2+} influx

Significance

Adenosine-to-inosine RNA editing generates various levels of editing in a developmental and spatiotemporal manner. This posttranscriptional process can diversify protein functions or levels through recoding codons or through affecting alternative splicing or noncoding RNA binding. In mammals, including humans, the editome contains millions of editing sites. This paper focuses on the functional and neurophysiological significance of L-type voltage-gated calcium channel $Ca_V1.3$ RNA editing. It is not only evolutionarily conserved across species but also tunable in response to training in learning and memory. The unexpected role that the $Ca_V1.3$ channel plays in hippocampal learning and memory was also revealed as a result of a combination of gain of function in biophysical properties arising from the loss of $Ca_V1.3$ RNA editing .

Author contributions: J.Z., S.N., H.H., and T.W.S. designed research; J.Z., S.N., S.Q.Z.Y., K.K.-K., M.C.L., J.H.K., and R.X.W. performed research; W.P.Y. contributed new reagents/analytic tools; J.Z., S.N., S.Q.Z.Y., K.K.-K., M.C.L., and S.S. analyzed data; J.Z., S.N., S.Q.Z.Y., H.H., and T.W.S. wrote the paper; and H.H. and T.W.S. provided supervision.

The authors declare no competing interest.

This article is a PNAS Direct Submission.

[1]To whom correspondence may be addressed. Email: phshhua@nus.edu.sg or phsstw@nus.edu.sg.

This article contains supporting information online at http://www.pnas.org/lookup/suppl/doi:10.1073/pnas.2203883119/-/DCSupplemental.

Published August 1, 2022.

is to increase neuronal excitability, enhance hippocampal plasticity that leads to strengthened late long-term potentiation (LTP), and, behaviorally, improved spatial learning and memory.

Results

$Ca_V1.3$ RNA Editing Is Evolutionarily Conserved from Zebrafish to Humans. There are millions of editing sites identified among different species. Conservation of RNA editing across species, such as isoleucine/valine (I/V) editing in the $K_V1.1$ channel and isoleucine/methionine (I/M) editing in the γ-aminobutyric acid type A receptor α3 receptor (GABRA3) (12, 13), points to their functional importance. We therefore examined brain $Ca_V1.3$ RNA editing across several mammalian species and discovered high conservation from zebrafish to humans (Fig. 1*A*), indicating that RNA editing of the $Ca_V1.3$ channel is evolutionarily conserved. The data suggest the neurophysiological importance of $Ca_V1.3$ RNA editing.

Genetic Deletion of the Editing-Site Complementary Sequence Completely Abolished RNA Editing of the $Ca_V1.3$ Channel. To address the twin questions of the physiological importance of $Ca_V1.3$ functional recoding of RNA editing and whether the loss of $Ca_V1.3$ editing results in greater or lower Ca^{2+} influx, we genetically targeted the mouse genome to remove the intronic editing-site complementary sequence (ECS) by homologous recombination (Fig. 1*B*). We have reported on the identity of the ECS (14), which forms the imperfect double-stranded stem structure that is essential for ADAR2 binding to initiate RNA editing. Replacing ECS with the loxP site by cre-recombinase disrupted the double-stranded stem structure that is critical for RNA editing. The success in generating the heterozygous $Ca_V1.3^{ECS/\Delta ECS}$ or homozygous $Ca_V1.3^{\Delta ECS/\Delta ECS}$ ($Ca_V1.3^{\Delta ECS}$) mice (Fig. 1 *C* and *D*) is clearly demonstrated by the retention of half the editing level in $Ca_V1.3^{ECS/\Delta ECS}$ and the total abolition of $Ca_V1.3$ RNA editing in $Ca_V1.3^{\Delta ECS}$ detected from whole brain tissue as compared to wild-type (WT) $Ca_V1.3^{ECS/ECS}$ ($Ca_V1.3^{ECS}$) mice (I/M: $Ca_V1.3^{ECS/ECS}$ 45.3% ± 1.352, $Ca_V1.3^{ECS/\Delta ECS}$ 24.32% ± 0.22, $Ca_V1.3^{\Delta ECS/\Delta ECS}$ 0.096% ± 0.096; Y/C: $Ca_V1.3^{ECS/ECS}$ 28.98% ± 0.4626, $Ca_V1.3^{ECS/\Delta ECS}$ 16.29% ± 0.2817, $Ca_V1.3^{\Delta ECS/\Delta ECS}$ 0.0% ± 0.0) (Fig. 1 *E* and *F*). Deletion of the intronic ECS sequence did not affect the production of $Ca_V1.3$ mRNA in the brain (Fig. 1*G*). We also did not detect any alterations in the C-terminal alternative splicing events of the $Ca_V1.3$ transcript (*SI Appendix*, Fig. S1 *A* and *B*). The gross phenotypes of $Ca_V1.3^{\Delta ECS}$ mice including hearing and vision were characterized to be normal, although the body weights of 3-month-old male mice were slightly heavier (*SI Appendix*, Fig. S2 *A*–*C*).

Lower RNA Editing Level in $Ca_V1.3$ IQ-Domain Detected in WT Mice after Water-Maze Training. Per our previous report (9), editing at the first site (*I/M*) of the $Ca_V1.3$ IQ-domain could be as high as 50% in the hippocampus. It has also been shown that I to M editing has more significant effects on open probability (Po) and calcium-dependent inactivation (CDI) of the $Ca_V1.3$ channel, while the functional effect of Y/C editing regarding Po and CDI is not obvious (9, 10). To study the functional importance of $Ca_V1.3$ RNA editing, we surmised that IQ-domain RNA editing in the $Ca_V1.3$ channel could be dynamically regulated during hippocampus-dependent learning and memory. Therefore, when we characterized the behavioral phenotypes of $Ca_V1.3^{\Delta ECS}$ mice using a Morris water maze, we first examined the editing level of the cornu ammonis 1 (CA1) region from untrained and trained WT $Ca_V1.3^{ECS}$ mice. Intriguingly, the $Ca_V1.3$ IQ-domain RNA editing levels in the CA1 region as well as the whole hippocampus were altered and were reduced, by 10%, after short-term water-maze training (Fig. 2*A* and *SI Appendix*, Fig. S3). This result indicates that the RNA editing of $Ca_V1.3$ channels is regulated during water-maze training and made us wonder how the loss of $Ca_V1.3$ RNA editing would affect hippocampus-dependent learning and memory and whether the net influx of Ca^{2+} ions would increase or decrease.

$Ca_V1.3^{\Delta ECS}$ Mice Exhibited Enhanced Spatial Learning and Memory in Morris Water Maze. Because $Ca_V1.3$ RNA editing was reduced after short-term water-maze training, we therefore hypothesized that hippocampal learning and memory could be affected in $Ca_V1.3^{\Delta ECS}$ mice. To test this hypothesis, we employed the Morris water maze behavioral tests in which the mice were guided by distal spatial cues to find a platform submerged in opaque water in a specified quadrant to evaluate learning ability. Probe tests, which involved removing the submerged platform, were performed on days 1, 5, and 12 to evaluate short-term, long-term, and remote memory, respectively. During the training trials on day 1, $Ca_V1.3^{\Delta ECS}$ and $Ca_V1.3^{ECS}$ mice had similar temporal latency in finding the platform. With further trainings from day 2 to day 4, both $Ca_V1.3^{ECS}$ and $Ca_V1.3^{\Delta ECS}$ mice showed clear improvements in their performances (Fig. 2*B*). However, $Ca_V1.3^{\Delta ECS}$ mice found the platform in a significantly shorter time latency as compared to WT mice, and the traces obtained on day 4 suggest that $Ca_V1.3^{\Delta ECS}$ mice had better performance in searching for the platform (Fig. 2*B*, *Inset*). One plausible explanation for the differences in water maze results could be differences in locomotor speed, but we found that the average swimming velocities of the $Ca_V1.3^{\Delta ECS}$ and $Ca_V1.3^{ECS}$ mice were similar (*SI Appendix*, Fig. S3). These results are indicative of $Ca_V1.3^{\Delta ECS}$ mice having better spatial learning ability. In addition, the $Ca_V1.3^{\Delta ECS}$ mice showed enhanced spatial memory because they spent significantly more time swimming in the target quadrant (the southeastern quadrant, where the platform was located during the training trials) in the probe tests. Of note, enhanced spatial memory of $Ca_V1.3^{\Delta ECS}$ mice was not only observed in the short-term memory (STM) probe test conducted 30 min after the last training trial on day 1 but also in the long-term memory (LTM) probe test performed on day 5, and significantly, it was maintained until the remote probe test on day 12 (Fg. 2C). To further corroborate the results of the memory probe tests, the $Ca_V1.3^{\Delta ECS}$ mice spent less time swimming in the diametrically opposite northwestern quadrant (Fig. 2*D*).

Enhanced Hippocampal Late LTP Underpinned Improved Spatial Learning and Memory in $Ca_V1.3^{\Delta ECS}$ Mice. The persistence of enhanced spatial learning and memory observed in the $Cav1.3^{\Delta ECS}$ mice suggests that RNA editing strongly influences the contribution of $Ca_V1.3$ channels in hippocampus-dependent learning and memory. The logical next step was to interrogate how LTP, a major cellular mechanism that underlies learning and memory, might be altered in $Ca_V1.3^{\Delta ECS}$ mice, especially in the CA1 area of the hippocampus. We examined persistent changes in the plasticity of the hippocampal CA3–CA1 synapses. Induced CA3–CA1 late LTP with a conventional high-frequency stimulation protocol using strong tetanus (STET) was recorded from both $Ca_V1.3^{\Delta ECS}$ and $Ca_V1.3^{ECS}$ mice with synaptic input S1 located at the Schaffer collateral projections. Single-pathway experiments were used for this study (Fig. 2*E*, *Inset*). A stable baseline was first recorded for a minimum of 30 min and STET was applied, which resulted in a long-lasting LTP until 180 min in $Ca_V1.3^{ECS}$ hippocampal slices. Next, we studied late LTP in $Ca_V1.3^{\Delta ECS}$ mice using the same paradigm,

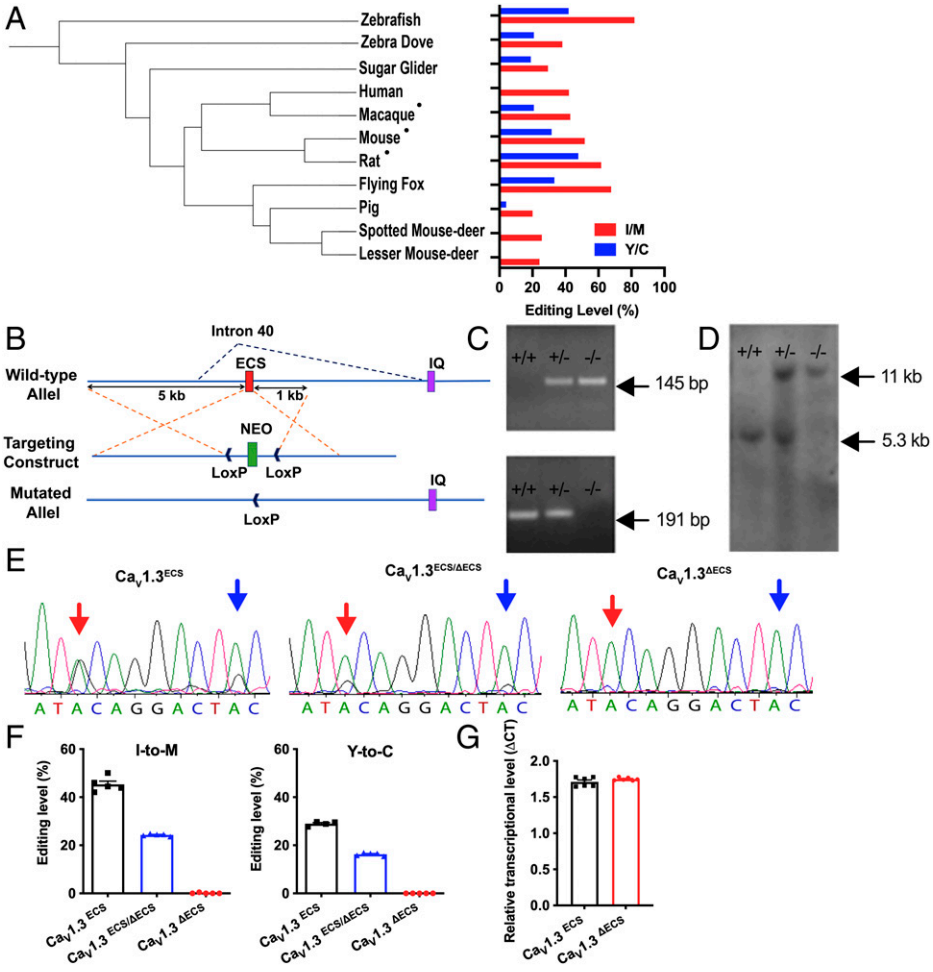

Fig. 1. Generation of Ca$_V$1.3$^{\Delta ECS}$ IQ-domain RNA editing knockout mice. (*A*) Polygenetic tree of animals tested for RNA editing events in the IQ-domain of Ca$_V$1.3 channels and quantification of editing levels in all tested species using brain tissues or the cDNA library (for humans). •Hippocampal tissues were used. (*B*) Schematic illustrating the knockout strategy with homologous recombination used to knock out intronic ECS in *Cacna1d*. (*C* and *D*) Genotyping by PCR and Southern blot analysis. PCR: 145 bp and 191 bp bands indicated the presence of ECS and ΔECS alleles, respectively; Southern blot analysis: 5.3 kb and 11 kb bands indicated the presence of ECS and ΔECS alleles, respectively. (*E*) Direct DNA sequencing of RT-PCR products from whole brain of Ca$_V$1.3^{ECS}, Ca$_V$1.3$^{ECS/\Delta ECS}$, and Ca$_V$1.3$^{\Delta ECS}$ mice. Red arrow: I/M editing site; blue arrow: tyrosine/cysteine (Y/C) editing site. (*F*) Percentage of editing calculated by measuring electropherogram heights for adenosine versus guanosine. No editing in Ca$_V$1.3$^{\Delta ECS}$ mice (n = 5), while Ca$_V$1.3-$^{ECS/\Delta ECS}$ mice (n = 5) exhibited half the editing level of Ca$_V$1.3^{ECS} mice (n = 5). *Left*: I/M editing site; *Right*: Y/C editing site. (*G*) Transcript level of *Cacna1d* quantified in Ca$_V$1.3$^{\Delta ECS}$ mice (n = 6) by RT-PCR was not different from that in Ca$_V$1.3^{ECS} mice (n = 6). Data represent means ± SEM. Scatters in bars indicate the number of analyzed animals. The two-tailed unpaired Student's t test was used for data in (*G*).

which resulted in an enhanced and more pronounced potentiation. In particular, the potentiation in Ca$_V$1.3 $^{\Delta ECS}$ mice was significantly higher than that in Ca$_V$1.3^{ECS} mice from 90 min onward, until 180 min (Fig. 2*E*). This showed that the Ca$_V$1.3$^{\Delta ECS}$ hippocampus after STET revealed enhanced late LTP, which is considered a cellular correlate of learning and memory.

Next, to determine whether a weaker form of LTP is affected in Ca$_V$1.3 $^{\Delta ECS}$ mice, we invoked early LTP using weak tetanus (WTET). When a WTET was delivered to hippocampal slices of Ca$_V$1.3^{ECS} and Ca$_V$1.3$^{\Delta ECS}$ mice, it resulted in early LTP in both cases. When the profiles of early LTP were compared between Ca$_V$1.3^{ECS} and Ca$_V$1.3 $^{\Delta ECS}$ hippocampal slices, they did not show any significant difference (*SI Appendix*, Fig. S4*A*). In addition, depotentiation and baseline recordings were also unaltered in Ca$_V$1.3$^{\Delta ECS}$ mice (*SI Appendix*, Fig. S4 *B* and *C*).

Loss of Ca$_V$1.3 RNA Editing Increased Ca^{2+} Influx into Hippocampal CA1 Pyramidal Neurons. While functional recoding via RNA editing of Ca$_V$1.3 enhanced learning and memory, to further understand the physiological and behavioral changes in Ca$_V$1.3$^{\Delta ECS}$ mice, we needed to first resolve the Ca$_V$1.3 IQ-domain editing paradox. The critical question was about whether the next Ca^{2+} influx into neurons was increased or decreased arising from the opposing effects of editing, on the one hand, to slow Ca$_V$1.3 Ca^{2+}-dependent inactivation to increase Ca^{2+} influx, and on the other, to reduce channel open probability to decrease Ca^{2+} influx. Total Ca^{2+} currents were therefore recorded directly from CA1 pyramidal neurons on the hippocampal slices, and the amount of low dihydropyridine (DHP)-sensitive current was isolated by first using low-dose nifedipine (1 μM) to substantively block primarily the Ca$_V$1.2 channels and then high-dose nifedipine (10 μM) to block the less-sensitive Ca$_V$1.3-mediated currents. The relative Ca$_V$1.3-mediated currents were determined by subtracting the peak Ca^{2+} currents recorded in 1 μM nifedipine from those recorded in 10 μM nifedipine at −10 mV. Therefore, as the Ca$_V$1.3 channel property has been modified in Ca$_V$1.3$^{\Delta ECS}$ mice, there is a strong likelihood that the difference in the observed low DHP-sensitive currents from WT would be contributed by Ca$_V$1.3 channels. We detected an approximately doubled Ca$_V$1.3 I_{Ca} in Ca$_V$1.3$^{\Delta ECS}$ CA1 neurons (Fig. 3*C*; Ca$_V$1.3^{ECS} −359.0 ± 62.61, Ca$_V$1.3$^{\Delta ECS}$ −655.2 ± 91.62; P = 0.0116). Therefore, we concluded that the loss of Ca$_V$1.3 RNA editing generated increased Ca^{2+} influx, suggesting that in the in vivo milieu, an increased open probability arising from the higher affinity of binding of calmodulin to the unedited Ca$_V$1.3 channel had a larger effect to increase Ca^{2+} conduction (10, 11). This result resolved the Ca$_V$1.3 editing paradox because RNA editing of the IQ-domain affects Ca^{2+} influx with opposing effects of CDI and channel open probability.

Enhanced Excitability of CA1 and CA3 Pyramidal Neurons in Ca$_V$1.3$^{\Delta ECS}$ Mice. The increased Ca^{2+} influx via unedited Ca$_V$1.3 channels provided the framework to uncover the underlying biophysical and molecular mechanisms for enhanced synaptic activity in the CA3–CA1 connections. DHP-sensitive voltage-gated calcium channels have been shown to contribute to low-voltage activated calcium current in

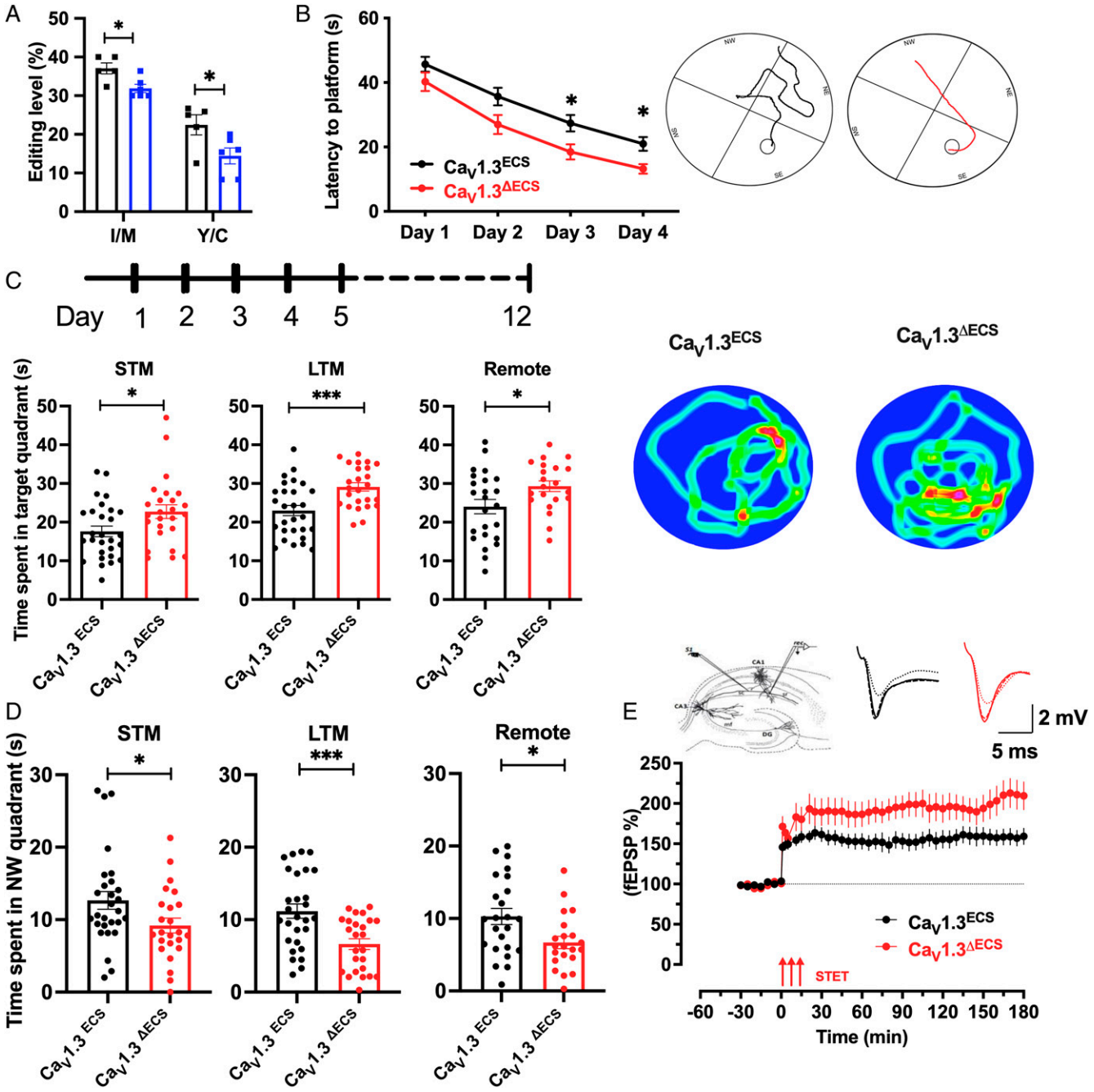

Fig. 2. Enhanced spatial learning and memory of Ca$_V$1.3$^{\Delta ECS}$ mice in Morris water maze. (*A*) Quantification of IQ-domain RNA editing levels at I-to-M and Y-to-C sites of Ca$_V$1.3 channels in hippocampal CA1 region from Ca$_V$1.3^{ECS} mice with (n = 6) and without (n = 5) water maze training. (*B*) Learning curve of Ca$_V$1.3^{ECS} (n = 28) and Ca$_V$1.3$^{\Delta ECS}$ mice (n = 25) during the Morris water maze training. Average latency to platform of training trials is presented. *Inset*: Representative swimming traces of Ca$_V$1.3^{ECS} and Ca$_V$1.3$^{\Delta ECS}$ mice exhibited the training trails on Day 4. (*C*) Time spent in target quadrant during probe tests. *Left*: STM probe test; *Middle*: LTM probe; *Right*: Remote probe test. *Inset*: Representative heat map of Ca$_V$1.3^{ECS} and Ca$_V$1.3$^{\Delta ECS}$ mice exhibits the time spent in each quadrant in LTM probe test. (*D*) Time spent in northwestern quadrant (opposite of the targeted southeastern quadrant) during STM (*Left*), LTM (*Middle*), and remote (*Right*) probe tests. (*E*) Late LTP in Ca$_V$1.3^{ECS} and Ca$_V$1.3 $^{\Delta ECS}$ mice with STET delivered in the stratum radiatum to stimulate Schaffer collateral fibers (*Left Inset*). STET in Ca$_V$1.3 $^{\Delta ECS}$ mice also resulted in a long-lasting LTP with Ca$_V$1.3 $^{\Delta ECS}$ mice showing a significantly higher percentage of potentiation than Ca$_V$1.3^{ECS} mice from 90 min onward until 180 min (Scale bar, 5 ms, 2 mV). Data represent means ± SEM. Scatters in bars indicate the number of analyzed animals. Two-way ANOVA with Sidak's multiple comparisons test was used for data in (*B*). Difference between genotypes, F (1, 50) = 10.77, P = 0.0019), *P < 0.05. The two-tailed unpaired Student's t test was used for data in (*A*, *C*, *D*); *P < 0.05, ***P < 0.001. The Mann–Whitney U test was used for data in (*E*) (90 min, P = 0.02; 120 min, P = 0.02; 180 min, P = 0.02).

hippocampal CA1 and CA3 pyramidal neurons (15, 16). Because Ca$_V$1.3 channels are activated close to the resting membrane potential (17) and unedited channels are also activated at a more hyperpolarized potential (9), our hypothesis was that Ca$_V$1.3$^{\Delta ECS}$ neurons would have more Ca$_V$1.3 channels available to depolarize the neurons at rest. Indeed, we recorded from Ca$_V$1.3$^{\Delta ECS}$ proximal CA1 pyramidal neurons and detected that the resting membrane potential (RMP) was depolarized by 5.70 ± 0.8209 mV (Fig. 3*D*; P < 0.0001), and the same difference was observed in distal CA3 pyramidal neurons (Fig. 3*G*; P < 0.0001). There was no difference in input resistance (*SI Appendix*, Fig. S5 *A* and *D*). To test whether the depolarized RMP could contribute to elevated membrane excitability, we determined the rheobase as an indicator of neuronal excitability and found consistently that Ca$_V$1.3$^{\Delta ECS}$ CA1 or CA3 neurons required lower injection of current to initiate action

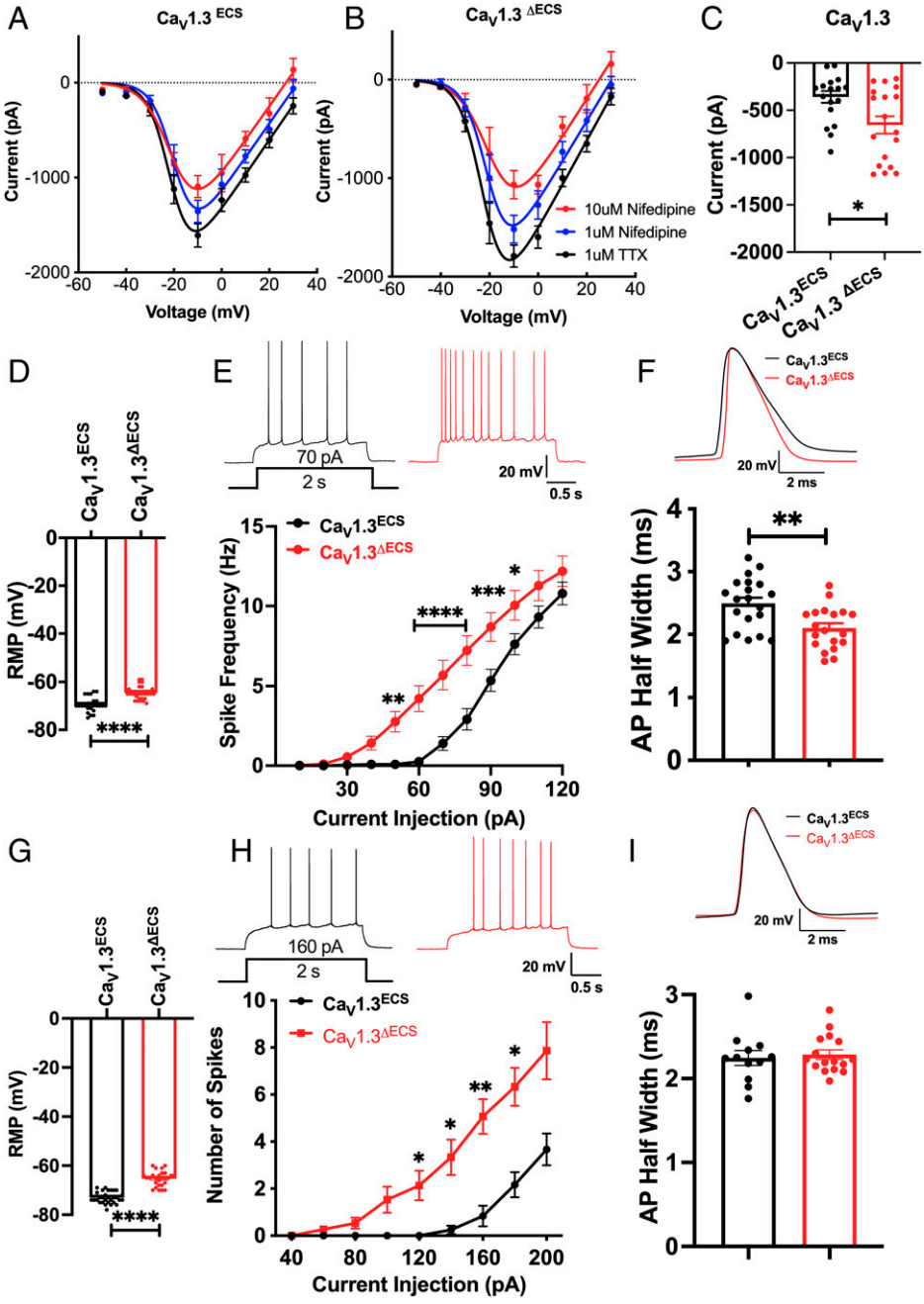

Fig. 3. Deletion of IQ-domain RNA editing increases $Ca_V1.3$ channel current and leads to enhanced neuronal excitability. (*A* and *B*) *I-V* curve of calcium current recorded from CA1 pyramidal neurons in hippocampal slices from $Ca_V1.3^{ECS}$ and $Ca_V1.3^{\Delta ECS}$ mice. The total Ca^{2+} currents were first recorded with 1uM TTX, and 1uM nifedipine was then applied to the bath solution to mostly block the high-affinity $Ca_V1.2$ channels. To isolate the low-affinity $Ca_V1.3$ currents, 10 μM nifedipine was subsequently added. (*C*) Increased amount of $Ca_V1.3$ currents calculated by the difference in peak Ca^{2+} currents recorded in 1uM versus 10 μM nifedipine at −10 mV. (*D*) Depolarized RMP of CA1 pyramidal neurons in $Ca_V1.3^{\Delta ECS}$ mice. (*E*) Representative traces of spike frequency (with 70 pA current injection for 2 s) and frequency–current curve showing spike frequency with current injection in CA1 pyramidal neurons. $n = 24$ and $n = 19$ for $Ca_V1.3^{ECS}$ and $Ca_V1.3^{\Delta ECS}$ mice, respectively. (*F*) Representative traces and quantification of CA1 pyramidal neurons AP half-width measured from average of the first AP in 5 trains with 10 s interval induced with 200 pA current injection. (*G*) Depolarized RMP of CA3 pyramidal neurons in $Ca_V1.3^{\Delta ECS}$ mice. (*H*) Representative traces of spike frequency (with 160 pA current injection for 2 s) and frequency–current curve showing spike frequency with current injection in CA3 pyramidal neurons of $Ca_V1.3^{ECS}$ ($n = 12$) and $Ca_V1.3^{\Delta ECS}$ mice ($n = 15$). (*I*) Representative traces and quantification of CA3 pyramidal neurons AP half-width measured from the average of the first AP in 5 trains with 10 s interval induced with 250 pA current injection did not show any difference between $Ca_V1.3^{ECS}$ and $Ca_V1.3^{\Delta ECS}$ mice. Data represent means ± SEM. Scatters in bars indicate the number of analyzed neurons. Two-way ANOVA with Bonferroni's multiple comparisons test was used for data in (*E* and *H*); the two-tailed unpaired Student's *t* test was used for analysis of data in all other panels. *$P < 0.05$; **$P < 0.01$; ***$P < 0.001$; ****$P < 0.0001$.

potential firings (Fig. 3*E*, CA1: $Ca_V1.3^{ECS}$ vs. $Ca_V1.3^{\Delta ECS}$, 70 pA vs. 40 pA, $F_{(1,32)} = 15.39$, $P = 0.0004$; Fig. 3*H*, CA3: $Ca_V1.3^{ECS}$ vs. $Ca_V1.3^{\Delta ECS}$, 140 pA vs. 80 pA, $F_{(1,14)} = 6.355$, $P = 0.0245$). To further characterize the increased excitability of CA1 and CA3 pyramidal neurons, the action potential duration (APD), action potential (AP) threshold, and spike frequency adaptation (SFA) ratio were recorded and analyzed. In $Ca_V1.3^{\Delta ECS}$ CA1 neurons, the APD was significantly narrower when compared to those recorded from $Ca_V1.3^{ECS}$ CA1 neurons (Fig. 3*F*; $P < 0.01$), and the threshold potential was significantly hyperpolarized (*SI Appendix*, Fig. S5*C*; $P < 0.05$). In CA3 neurons, both the APD and AP threshold were, however, comparable between $Ca_V1.3^{\Delta ECS}$ and $Ca_V1.3^{ECS}$ mice (Fig. 3*I* and *SI Appendix*, Fig. S5*F*). The SFA ratio detected from both $Ca_V1.3^{\Delta ECS}$ CA1 and CA3 neurons was lower, suggesting that there would be less adaptation during firing (*SI Appendix*, Fig. S5 *B* and *E*).

Increased Large-Conductance Ca2+-activated (BK) Potassium Channel Activation Contributes to Enhanced Neuronal Excitability by Close Coupling with CaV1.3 Channel in CA1 Pyramidal Neurons. While the biophysical property of the unedited $Ca_V1.3$ channels provides an explanation for membrane excitability, we also observed reduced AP width and firing adaptation. Therefore, we next queried whether the increased influx of Ca^{2+} observed in $Ca_V1.3^{\Delta ECS}$ CA1 neurons may functionally couple with Ca^{2+}-activated potassium channels to increase action potential firings. A candidate to test this hypothesis is the BK channel, as it has been shown that BK channels underlie repolarization and fast afterhyperpolarization to support high-frequency AP firing in hippocampal neurons (18). Furthermore, the reported proximal clustering of $Ca_V1.3$ and BK channels promotes the activation of the BK channel at low voltage and therefore may serve to regulate neuronal excitability in the rat hippocampus (19). Therefore, we performed whole-cell patch-clamp

electrophysiological recordings with 1μM tetrodotoxin (TTX) and 100 nM iberiotoxin (IbTX, BK channel antagonist) to isolate the outward (I_{BK}) K^+ currents. With the presence of 5 mM ethylene glycol tetraacetic acid (EGTA) in the internal solution, we observed larger outward K^+ currents ($Ca_V1.3^{ECS}$: 2104.6 ± 410.7 pA; $Ca_V1.3^{\Delta ECS}$: 3608.5 ± 645.7 pA) (Fig. 4*A* and *SI Appendix*, Fig. S6 *A* and *B*) that displayed a transient peak sensitive to IbTX-blocking in the $Ca_V1.3^{\Delta ECS}$ CA1 neurons. The IbTX-sensitive currents at 70 mV were ~twofold larger as recorded from the CA1 neurons of the $Ca_V1.3^{\Delta ECS}$ mice ($Ca_V1.3^{ECS}$: 935.2 ± 293.2 pA; $Ca_V1.3^{\Delta ECS}$: 1888 ± 287.5 pA; $P = 0.0043$) (Fig. 4*C*). Therefore, we surmised that this transient peak represented the fast activation of the BK channel, triggered due to a close functional coupling with the $Ca_V1.3$ channels. To address this possibility, we used an internal solution with 10 mM 1,2-bis(o-aminophenoxy)ethane-N,N,N′,N′-tetraacetic acid) (BAPTA), a fast Ca^{2+} chelator, to disrupt the close proximity coupling between $Ca_V1.3$ and the BK channel. Indeed, the IbTX-sensitive currents were mostly abolished in both mice (Fig. 4 *B* and *C* and *SI Appendix*, Fig. S6 *A* and *B*). To corroborate this finding, we investigated whether blocking the BK channels would affect the APD and the SFA and found that in the presence of IbTX, the APD became significantly wider and that the SFA ratio was increased for both $Ca_V1.3^{\Delta ECS}$ and $Ca_V1.3^{ECS}$ neurons (Fig. 4 *D* and *E* and *SI Appendix*, Fig. S6 *C–F*).

Enhanced Synaptic Transmission at CA3–CA1 Synapses in $Ca_V1.3^{\Delta ECS}$ Mice. After assessing the enhanced excitability of $Ca_V1.3^{\Delta ECS}$ CA1 and CA3 pyramidal neurons due to a gain of function as a result of the loss of editing of the $Ca_V1.3$ channels, we probed how synaptic transmission is affected at the CA3–CA1 synapses. To investigate whether presynaptic activity or postsynaptic responses might be involved, miniature excitatory postsynaptic currents (mEPSCs) of CA1 pyramidal neurons were recorded at −70 mV in acute adult hippocampal slices prepared from both $Ca_V1.3^{\Delta ECS}$ and $Ca_V1.3^{ECS}$ mice (Fig. 5*A*). Because $Ca_V1.3$ channels are mostly expressed on the dendrites and soma of neurons, we were surprised by the significant increase in mEPSC frequency, as this result suggests the enhanced presynaptic release of neurotransmitters (Fig. 5*B*). Because little is known about how $Ca_V1.3$ channels contribute to hippocampal LTP (20–22), the increase in mEPSC amplitude, which suggests enhanced postsynaptic reception, was also intriguing (Fig. 5*C*). To further characterize the underlying postsynaptic mechanism, we determined the α-amino-3-hydroxy-5-methyl-4-isoxazolepropionic acid receptor (AMPAR)/N-methyl-D-aspartate receptor (NMDAR) ratio, because this result showed the relative expression of AMPA and NMDA receptors at the postsynapse. With stimulation electrode located at the Schaffer collaterals, the AMPAR/NMDAR ratio recorded from CA1 pyramidal neurons was higher in the $Ca_V1.3^{\Delta ECS}$ mice, suggesting that there were relatively more AMPA receptors present in the postsynaptic membranes (Fig. 5*D*). The increased Ca^{2+} current through the $Ca_V1.3$ channel and the enhanced activity of CA1 neurons are likely to promote the trafficking and insertion of the AMPA receptor to the postsynaptic terminals, as previously reported (23).

Up-Regulated Activation of Inhibitory Cannabinoid Type 1 Receptor (CB1R) for Homeostatic Feedback. Apart from increased postsynaptic responses in the CA3–CA1 synapse, we also found that paired-pulse ratios (PPRs) were significantly higher at short interstimulus intervals in $Ca_V1.3^{\Delta ECS}$ hippocampus (Fig. 5*E*). Increased PPR could be associated with inhibited presynaptic neurotransmitters release upon the first pulse, while the local accumulation of Ca^{2+} leads to an enhanced release when the second pulse arrives. To uncover the explanation for increased PPR, we evaluated the inhibitory retrograde endocannabinoid signaling pathway (24). With a 50 ms interpulse interval, the PPR in the $Ca_V1.3^{\Delta ECS}$ hippocampus was significantly reduced to a level similar to that of $Ca_V1.3^{ECS}$ by 10 μM CB1 receptor antagonist AM251 (Fig. 5*F*). This finding suggests that there was enhanced basal activation of CB1R in the $Ca_V0.3^{\Delta ECS}$ CA1 presynapse. Therefore, the increased PPR in the $Ca_V1.3^{\Delta ECS}$ CA3–CA1 connection could be due to the disinhibition of presynaptic release after the first pulse so that the second pulse generates a larger response. It is possible that at the basal level, increased activation of CB1R in $Ca_V1.3^{\Delta ECS}$ mice leads to an increase in tonic Gβγ inhibition of Ca_V2 channels to suppress the neurotransmitter release (25–30). Upon the first stimulating pulse, due to depolarization of the membrane potentials, the inhibition of Ca_V2 by Gβγ was relieved and was further relieved in the $Ca_V1.3^{\Delta ECS}$ mice. The increased amount of presynaptic calcium influx then accumulated at the presynaptic terminal to trigger an increase in the synaptic release of the neurotransmitter upon the second pulse.

Increased Dendritic Arborization and Spine Density of CA1 Pyramidal Neurons Support Their Enhanced Synaptic Activity. Since the Ca^{2+} ion as a signaling molecule is important for changes in dendritic structure and arborization, we scrutinized alterations in the dendritic arborization and spine number of CA1 pyramidal neurons. To visualize a CA1 pyramidal neuron in a hippocampal slice, a single neuron was dialyzed with Alexa fluorescent 488 dye via an attached patch pipette. The labeled neurons were subject to Sholl analysis for morphological characterizations. In congruence with enhanced synaptic activity, we observed increased dendritic intersections in the basal dendrites of CA1 pyramidal neurons of $Ca_V1.3^{\Delta ECS}$ mice (Fig. 5*G*; $P = 0.0006$). In addition, the dendritic intersections of the apical dendrites were also significantly higher in $Ca_V1.3^{\Delta ECS}$ CA1 pyramidal neurons (Fig. 5*H*; $P = 0.0395$). Enumeration of the spine density revealed that $Ca_V1.3^{\Delta ECS}$ CA1 pyramidal neurons had a higher density of spines in the basal dendrites (*SI Appendix*, Fig. S7).

Changes in Ca^{2+} Signaling Pathways in $Ca_V1.3^{\Delta ECS}$ and $Ca_V1.3^{ECS}$ CA1 Neurons after Spatial Learning. Our follow-up question was about how a larger Ca^{2+} influx observed in $Ca_V1.3^{\Delta ECS}$ mice may signal to contribute to enhanced hippocampal synaptic plasticity. Ca^{2+} influx through L-type calcium channels is known to drive local Ca^{2+}/calmodulin-dependent protein kinase II (CaMKII) aggregation and trigger nuclear signaling for cAMP-response element binding protein CREB-dependent gene expression (31, 32). Here, we predicted that the increased Ca^{2+} current density would elevate the accumulation of CaMKII and downstream CREB activity in $Ca_V1.3^{\Delta ECS}$ mice during water-maze training. To substantiate this possibility, we measured the expression and phosphorylation level of CaMKII and CREB in CA1 regions from both untrained mice and the Morris water maze–trained $Ca_V1.3^{\Delta ECS}$ and $Ca_V1.3^{ECS}$ mice after the STM probe test (Fig. 6*A*). First, we detected increased levels of phosphorylated-αCaMKII and βCaMKII (threonine286) as well as nonphosphorylated βCaMKII in the trained $Ca_V1.3^{ECS}$ and $Ca_V1.3^{\Delta ECS}$ mice. Of note, the level of p-αCaMKII was significantly higher in trained $Cav1.3^{\Delta ECS}$ mice as compared to that in trained $Ca_V1.3^{ECS}$ mice (Fig. 6*B*). The increased phosphorylation of αCaMKII would support enhanced synaptic transmission in a kinase-dependent manner, while the increased βCaMKII would

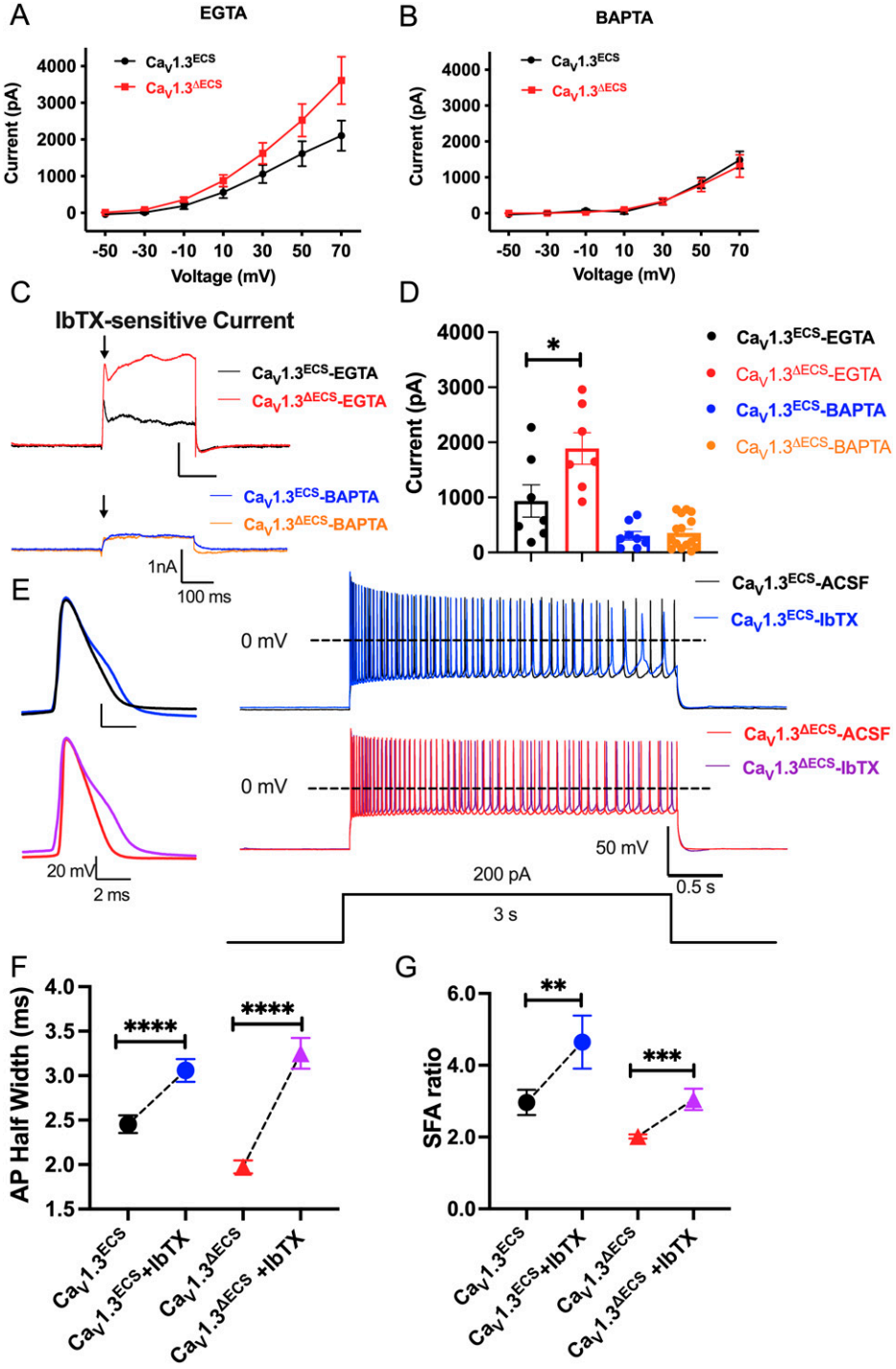

Fig. 4. Increased BK current in $Ca_V1.3^{\Delta ECS}$ mice due to close coupling with $Ca_V1.3$ channel affects APD and SFA in CA1 neurons. (*A*) *I-V* curve of I_K currents recorded with EGTA in the pipette solution from CA1 pyramidal neurons in hippocampal slices from $Ca_V1.3^{ECS}$ (n = 7) and $Ca_V1.3^{\Delta ECS}$ (n = 8) mice. (*B*) *I-V* curve of I_K currents recorded with BAPTA in the pipette solution from CA1 pyramidal neurons in hippocampal slices from $Ca_V1.3^{ECS}$ (n = 13) and $Ca_V1.3^{\Delta ECS}$ (n = 22) mice. (*C*) Representative trace quantification of subtracted IbTX-sensitive I_{BK} in CA1 pyramidal neurons with the presence of EGTA or BAPTA in the internal solution. (*D*) Quantification of IbTX-sensitive I_{BK} in CA1 pyramidal neurons with the presence of EGTA or BAPTA in the internal solution. (*E*) Representative traces of the first AP and trains of APs induced by 200 pA current injection for 3 s before and after IbTX treatment in CA1 pyramidal neurons. (*F*) Quantification of AP half-width before and after 100 nM IbTX treatment from $Ca_V1.3^{ECS}$ (n = 20) and $Ca_V1.3^{\Delta ECS}$ mice (n = 14). (*G*) Quantification of SFA ratio before and after IbTX treatment in $Ca_V1.3^{ECS}$ (n =15) and $Ca_V1.3^{\Delta ECS}$ mice (n = 21). Data represent means ± SEM. Scatters in bars indicate the number of analyzed neurons. The two-tailed unpaired Student's t test was used for analysis of data in (*D*); the two-tailed paired Student's t test was used for analysis of data in (*F* and *G*). *P < 0.05; **P < 0.01; ***P < 0.001; ****P < 0.0001.

contribute toward an activity-induced kinase-independent role in the maintenance of dendritic spine architecture (33). Second, for CREB activity, we detected a significant increase of the p-CREB level in the trained $Ca_V1.3^{\Delta ECS}$ mice as compared to the untrained $Ca_V1.3^{\Delta ECS}$ mice and the trained $Ca_V1.3^{ECS}$ mice (Fig. 6*C*). Considering that hippocampal tissues were harvested 30 min after the short-term probe test, it may have still been too early to capture changes of CREB activity in $Ca_V1.3^{ECS}$ mice. Therefore, the elevated level of p-CREB indicated that the Ca^{2+}-triggered signaling to the nucleus is promoted in $Ca_V1.3^{\Delta ECS}$ mice. Third, we also found that in both $Ca_V1.3^{ECS}$ and $Ca_V1.3^{\Delta ECS}$ mice, the Morris water-maze training elevated the expression of nonphosphorylated synapsin 1 (Syn-1) protein (Fig. 6*D*). Syn-1 has been reported to be associated with activity-induced vesicle release at presynaptic terminals (34). Syn-1 regulates the number of synaptic vesicles at the active zone in a bidirectional manner. The level of Syn-1 is positively associated with the number of vesicles at the presynaptic terminals, while the phosphorylation of Syn-1 removes the vesicles from the active zone (34). Parallel to what we observed for CaMKII, the level of Syn-1 was approximately 1.75-fold higher in trained $Ca_V1.3^{\Delta ECS}$ mice as compared to trained $Ca_V1.3^{ECS}$ mice, supporting the enhanced synaptic activity during learning in $Ca_V1.3^{\Delta ECS}$ mice. As shown earlier that the editing level of $Ca_V1.3$ was reduced after the STM probe test in the $Ca_V1.3^{ECS}$ mice, this reduction of editing would allow more Ca^{2+} influx and therefore trigger downstream signaling of CaMKII and CREB proteins. Although the editing level of $Ca_V1.3$ channels was

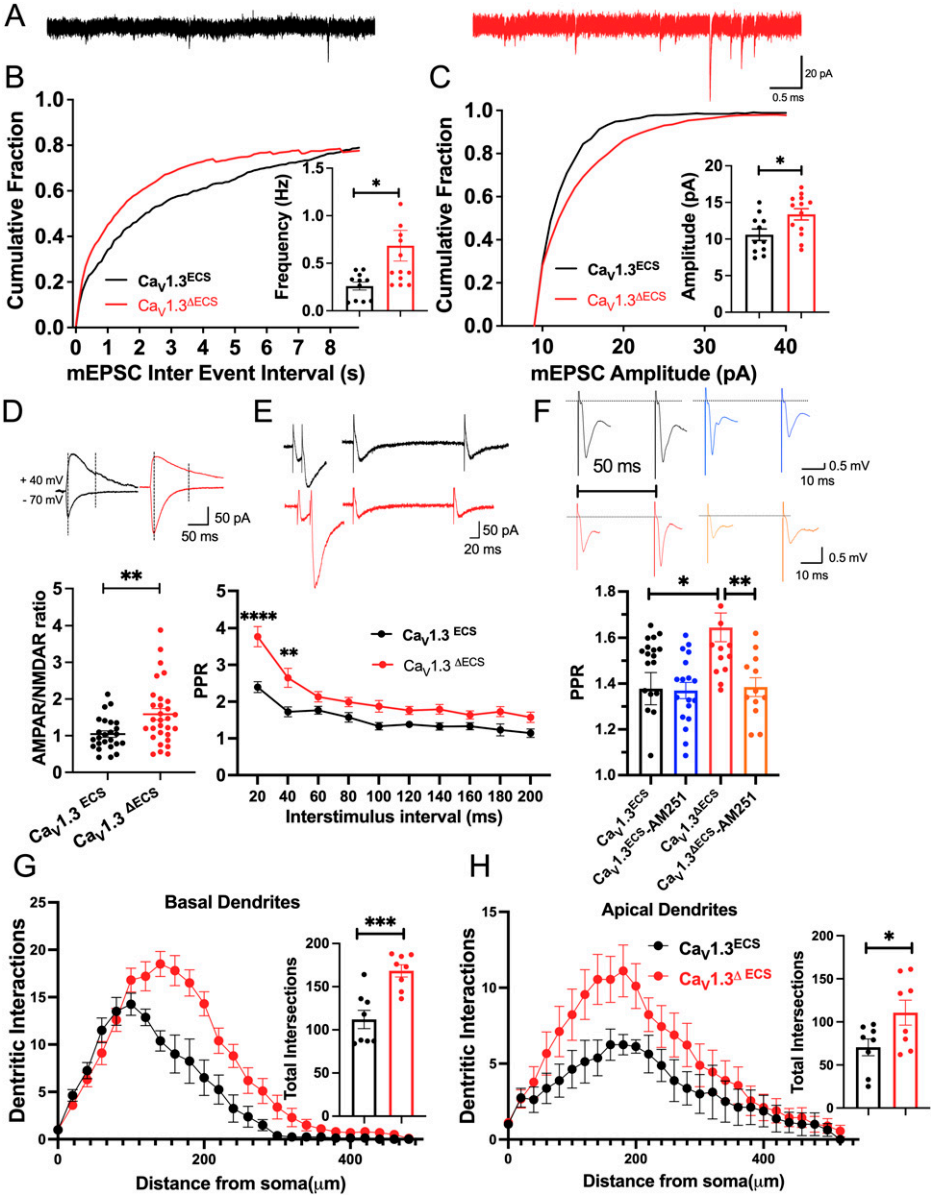

Fig. 5. Increased synaptic transmission and dendritic intersections of CA1 pyramidal neurons in $Ca_V1.3^{\Delta ECS}$ mice. (*A*) Representative trace of mEPSCs recorded in CA1 pyramidal neurons from $Ca_V1.3^{ECS}$ (black) and $Ca_V1.3^{\Delta ECS}$ mice (red) (Scale bar, 0.5 s and 20 pA). (*B* and *C*) Histogram and cumulative fraction of the interevent interval and amplitude of mEPSCs, $n = 11$ and $n = 13$ for $Ca_V1.3^{ECS}$ and $Ca_V1.3^{\Delta ECS}$ mice. (*D*) Representative traces and quantification of AMPAR/NMDAR ratio calculated by estimating the respective AMPAR and NMDAR component at +40 mV based on their different time courses (Scale bar, 50 ms and 50 pA). (*E*) Representative traces and quantification of PPR recorded in CA1 pyramidal neurons with stimulus located in the stratum radiatum at various interpulse intervals from 20 to 200 ms. $n = 30$ and $n = 24$ for $Ca_V1.3^{ECS}$ and $Ca_V1.3^{\Delta ECS}$ mice, respectively (Scale bar, 20 ms and 50 pA). (*F*) Quantification of PPR measured from the slope of fEPSPs with stimulus located in the stratum radiatum at a 50 ms interpulse interval before and after applying CB1R antagonist AM251 (10 μM). $n = 20$ and $n = 15$ for $Ca_V1.3^{ECS}$ and $Ca_V1.3^{\Delta ECS}$ mice, respectively, before AM251 treatment. $n = 18$ and $n = 12$ for $Ca_V1.3^{ECS}$ and $Ca_V1.3^{\Delta ECS}$ mice, respectively, after applying AM251. (*G* and *H*) Quantification of basal and apical dendritic intersections of CA1 pyramidal neurons. Total intersections were counted. $n = 8$ and $n = 8$ for $Ca_V1.3^{ECS}$ and $Ca_V1.3^{\Delta ECS}$ mice, respectively. Data represent means ± SEM. Scatters in bars indicate the number of analyzed neurons or slices. Two-way ANOVA with Bonferroni's multiple comparisons test was used for data in (*E*); the two-tailed unpaired Student's *t* test was used for analysis of data in all other panels. $^*P < 0.05$; $^{**}P < 0.01$; $^{***}P < 0.001$.

down-regulated after training, the expression levels of $Ca_V1.3$ channels in the CA1 region and the editing regulator of ADAR2 such as Ser/Arg (SR)-rich splicing factor 9 (SRSF9) was unaltered (Fig. 6*E*).

Discussion

While the $Ca_V1.3$ channel is expressed in multiple organs, RNA editing of its IQ-domain is restricted to neurons of the central nervous system. Here, we provide evidence that mammalian RNA editing could be adaptive and that editing recoding has functional, physiological, and behavioral importance. This notion is supported by, first, the evolutionary conservation of $Ca_V1.3$ IQ-domain RNA editing across various mammalian species, from zebrafish to humans. Second, enhanced hippocampal plasticity, learning, and memory observed in mice with a total loss of $Ca_V1.3$ RNA editing suggest that a dynamic regulation of $Ca_V1.3$ RNA editing would affect spatial learning and memory. Moreover, these mice exhibited an unexpected gain of function because unedited $Ca_V1.3$ channels support a larger Ca^{2+} influx into the neurons. This result resolved the $Ca_V1.3$ editing paradox because RNA editing of the IQ-domain affects CDI and channel open probability, two calmodulin-dependent processes that elicit opposing effects on Ca^{2+} influx.

Functional Recoding of $Ca_V1.3$ RNA Editing Results in Decreased Ca^{2+} Influx. The $Ca_V1.3$ RNA editing paradox revolves around the opposing effects of editing to slow Ca^{2+}-dependent inactivation to increase Ca^{2+} influx (9), while on the contrary, editing lowers the affinity of the binding of apocalmodulin to the $Ca_V1.3$ IQ-domain to lead to reduced open probability and less Ca^{2+} influx (10, 11). Here, we observed increased $Ca_V1.3$ current in CA1 pyramidal neurons in $Ca_V1.3^{\Delta ECS}$ mice, indicating that with the deletion of RNA editing, the unedited $Ca_V1.3$ channel allowed a larger entry of Ca^{2+}. This result resolved the editing paradox, and although unedited $Ca_V1.3$ channels displayed more robust CDI, the effect of increased open probability was more dominant. The increased $Ca_V1.3$ Ca^{2+} currents, coupled with the more hyperpolarized activation of the unedited $Ca_V1.3$ channel, led to a more depolarized resting membrane potential, which served as the basis of the enhanced excitability of CA1 and CA3 neurons.

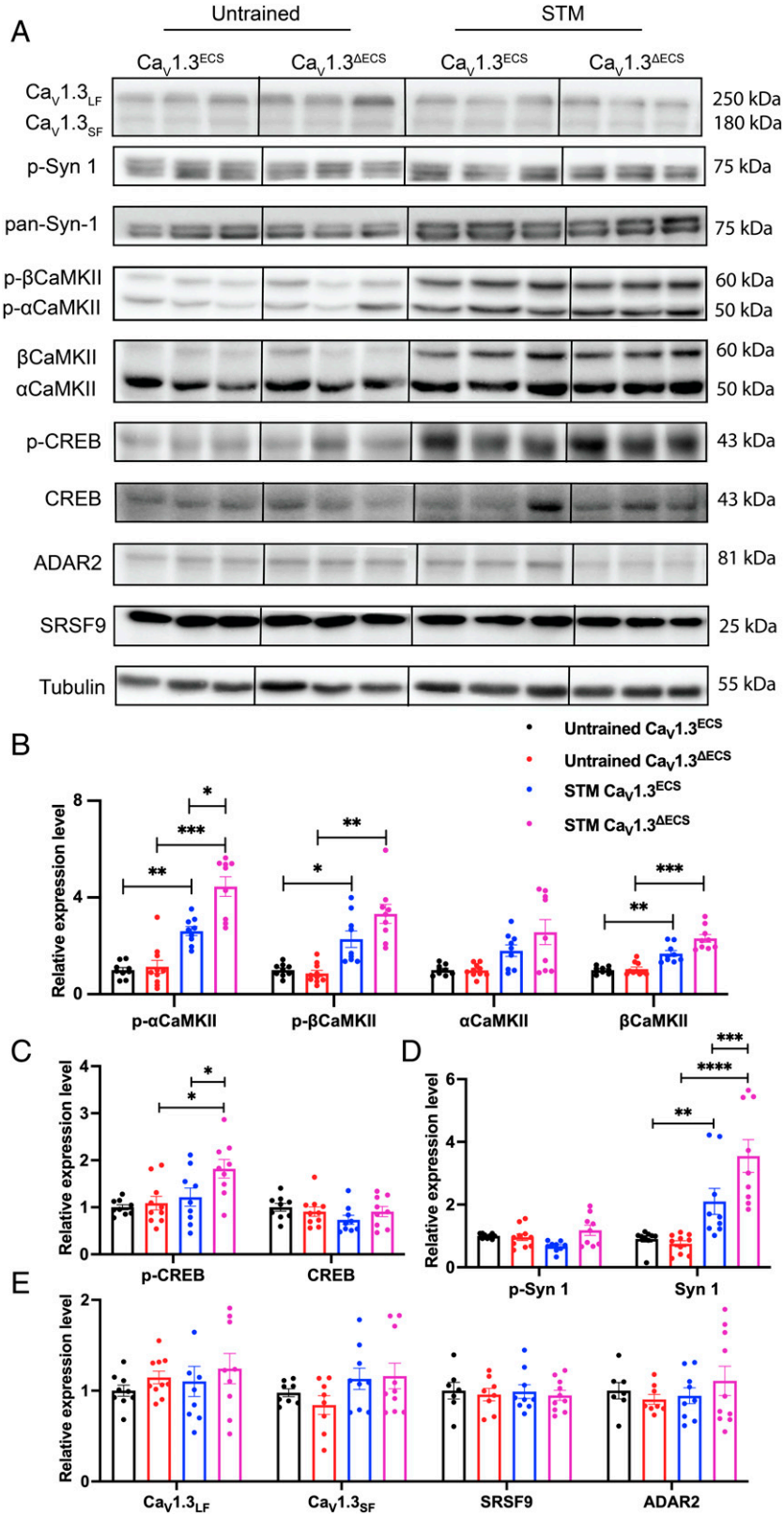

Fig. 6. Regulation of Ca^{2+}-dependent signaling pathway after Morris water maze and the dynamics and conservation of RNA editing in $Ca_V1.3$ channels. (*A*–*E*) Immunoblotting analysis of plasticity-related proteins in hippocampal CA1 from untrained $Ca_V1.3^{ECS}$ and $Ca_V1.3^{\Delta ECS}$ mice as well as those trained for four trials and tested with STM probe test. Quantification of relative expression level of p-CaMKII and CaMKII (*B*); p-CREB and CREB (*C*); p-Syn-1 and Syn-1 (*D*); $Ca_V1.3_{LF}$ (long-form splicing variant $Ca_V1.3_{42}$ with predicted size of 250 kDa), $Ca_V1.3_{SF}$ (short-form splicing variants $Ca_V1.3_{42a}$, $Ca_V1.3_{43S}$ and $Ca_V1.3_{43S2}$ with predicted size around 180 kDa), SRSF9, and ADAR2 (*E*) with and without water-maze training in $Ca_V1.3^{ECS}$ and $Ca_V1.3^{\Delta ECS}$ mice. (*B*–*E*) Data represent means ± SEM. Scatters in bars indicate the number of analyzed animals. Two-way ANOVA with Bonferroni's multiple comparisons test was used. Mixed-effects analysis (type III) of genotype and training: p-CaMKII and CaMKII ($F(1.767, 15.90) = 51.9$, $P < 0.0001$), p-CREB and CREB ($F(2.766, 24.89) = 3.690$, $P = 0.0278$), and p-Syn-1 and Syn-1 ($F(3, 27) = 12.49$, $P < 0.0001$); *$P < 0.05$; **$P < 0.01$; ***$P < 0.001$; ****$P < 0.0001$.

Close Coupling of $Ca_V1.3$ and BK Channel in CA1 Pyramidal Neurons Determines APD. In this study, we demonstrated that mice with a deletion of RNA editing in the $Ca_V1.3$ channel exhibited enhanced excitability of CA1 and CA3 pyramidal neurons. Increased firing with current injection, depolarized RMP, and lower SFA were observed in both CA1 and CA3 neurons in the $Ca_V1.3^{\Delta ECS}$ hippocampus. We also found that narrowed APD was only present in CA1 pyramidal neurons but not in CA3 pyramidal neurons. Moreover, treatment using IbTX was able to broaden APD in CA1 neurons. This difference between CA1 and CA3 pyramidal neurons could be due to the different types of BK channels expressed in those neurons. In CA1 neurons, inactivating the BK channel with the accessory β_2-subunit reveals fast gating kinetics, is IbTX-sensitive, and regulates

repolarization of AP and spike duration (35, 36). For this type of BK channel, its effect on APD is strongly associated with the amount of Ca^{2+} influx. However, in CA3 neurons, high expression of the β_4 subunit detected by in situ hybridization has been reported, and the data are corroborated in the Allan Brain Atlas (mouse.brain-map.org/gene/show/37365). These β_4-containing noninactivating BK channels are expressed dominantly on the CA3 neuronal membrane, and they are slow-gating and IbTX-insensitive (37). It has also been reported that in CA3 neurons, BK channels modulate APD through the interaction of the β_4 subunit and the Fragile X mental retardation protein (38). Therefore, an increased amount of inactivating BK current in CA1 neurons contributes to the narrowed APD and enhanced firing, whereas the increased excitability of CA3 pyramidal neurons is mainly associated with changes of membrane properties such as depolarized RMP. In addition, there are also multiple mechanisms that regulate BK channel activity such as alternative splicing, β-subunit composition, posttranslational modification, and the Ca^{2+} source that coalesce to underlie the differences in BK channel properties in various types of neurons (18, 39).

Enhanced Synaptic Activity and CB1R Homeostatic Feedback. It is intriguing that on the one hand, both the frequency and amplitude of mEPSC were increased in $Ca_V1.3^{\Delta ECS}$ CA1 pyramidal neurons that are indicative of enhanced neurotransmitter release and response. On the other hand, the PPR was also higher with up-regulated activation of inhibitory CB1R in the $Ca_V1.3^{\Delta ECS}$ CA3–CA1 connection that would lead to a reduced release probability at the presynaptic terminal. Because the frequency of mEPSCs could be affected by multiple factors including the release probability of presynaptic terminals (40), the surface expression of AMPA receptors (23, 41), and the number and morphology of dendritic spines (42), we surmise that the increased frequency of mEPSC we observed here could be contributed by one factor or a combination of these factors. The up-regulation of endocannabinoid activity could be a postsynaptic homeostatic feedback signal to scale down synaptic neurotransmission for preventing hyperactivity. Nonetheless, the net effect we observed in $Ca_V1.3^{\Delta ECS}$ mice was enhanced synaptic transmission.

Functional Importance of $Ca_V1.3$ RNA Editing. RNA editing, a posttranscriptional modification, could deaminate an adenosine in the noncoding RNA to affect transcript stability, binding affinity, or splicing and in coding exons to be recoded with synonymous or nonsynonymous change in the amino acid codon. Recoding of exons leads to diversification of protein function in response to various environmental or physiological conditions. The functional outcomes of $Ca_V1.3$ RNA editing provide evidence of its importance in response to physiological or pathological stimuli. Our results agree well with previous published reports on the functional importance of RNA editing, as shown in the conditional knockout mouse model of the glutamate recepor subunit B (GluR-$B^{+/\Delta ECS}$) and the knock-in mouse models expressing an unedited /fully edited 5-HT_{2C} receptor. However, because the glutamine/arginine (Q/R) editing site was almost fully edited, the homozygous deletion of GluR-B ECS led to early seizure-related death in mice. Therefore, the model used for functional study was the heterozygous GluR-$B^{+/\Delta ECS}$ or rescued $ADAR2^{-/-}$/GluR-$B^{R/R}$ mice. Reduced Q/R editing in the hippocampus led to an epileptic phenotype due to the retained Ca^{2+} permeability of unedited GluR-B receptors (6), while a complete loss of GluR-B editing was a gain of function of Ca^{2+} permeability. While the 5-HT_{2C} R-INI knockout mice did not show any obvious phenotype, the $5HT_{2C}$ R-VGV knock-in mice showed a severe reduction in body fat as a result of the constitutive activation of the sympathetic nerve and increased energy expenditure (7). As for the $GABA_A$ receptor and $K_V1.1$ channel, because their stem–loop structure that is formed between ECS and the editing site lies within the coding region, until now, transgenic mouse models specifically targeting RNA editing are not available (12, 13). As such, to the best of our knowledge, the $Ca_V1.3^{\Delta ECS}$ mice are the first surviving ECS knockout of ion channels or receptors that has a gain of function phenotype with enhanced spatial learning and memory and neuronal plasticity. To more precisely characterize other neurological functions, a $Ca_V1.3$ ECS conditional knockout model would have to be generated in the future. Nonetheless, the $Ca_V1.3^{\Delta ECS}$ mice uncovered a role of $Ca_V1.3$ channels in hippocampal-dependent learning and memory. Of note, the knockout mouse model of the $Ca_V1.3$ channel did not show any deficit in spatial learning (21). However, it seems that the roles of the $Ca_V1.3$ channel in neurocognitive functions were revealed through a gain of function of channel activity. Gain of function of the $Ca_V1.3$ channel has been associated with Parkinson's disease (PD) and various neuropsychiatric disorders. The $Ca_V1.3$ channel serves an important role in supporting the spontaneous pacemaking activity of substantia nigra pars compacta (SNc) neurons, which after degeneration and death lead to PD. L-type channel blocker DHPs have been found to be protective in PD mouse and nonhuman primate models (43–45). The stimulation of $Ca_V1.3$ channels by BayK8644 in vivo has induced depression-like behavior (46), while a lack of $Ca_V1.3$ leads to anti-depressive behavior (47). Multiple gain-of-function mutations in *CACNA1D* have also been reported in patients with sporadic autism and intellectual disability (48–50) as well as patients with primary aldosteronism and those with neurodevelopmental deficits and seizures at an early age (51). More intriguingly, recent studies have also reported significantly reduced A-to-I RNA editing of $Ca_V1.3$ channels from 14 to 8% in the hippocampus from patients with AD compared to healthy control samples (52, 53). This is likely associated with the down-regulation of ADAR expression in patients with AD. Moreover, the expression level of $Ca_V1.3$ channels has also been shown to be lower in patients with AD (54, 55). Due to the complexity of AD pathology, it is still largely unknown whether the down-regulation of editing is detrimental, compensatory, or neutral. Here, the enhanced hippocampal plasticity and spatial learning and memory observed from this gain-of-function model of $Ca_V1.3^{\Delta ECS}$ mice provide insights into the roles of the $Ca_V1.3$ channel and the importance of fine-tuning calcium channel activity to regulate Ca^{2+} influx for optimal functional outcomes. In this study, we have focused particularly on spatial learning and memory. Further investigations would be needed to reveal whether other memory systems such as fear memory and associative memory would be affected in $Ca_V1.3^{\Delta ECS}$ mice. The wider implications of $Ca_V1.3$ RNA editing in other brain functions await discovery.

The $Ca_V1.3$ channel is also known to be important for neurogenesis and the differentiation of the hippocampal dentate gyrus (DG) (56). The $Ca_V1.3^{-/-}$ mice exhibited impaired DG neurogenesis, reduced DG volume, and survival of newly differentiated neurons. As reported, the $Ca_V1.3^{-/-}$ mice failed to discriminate the differences in object location during the object location memory test, and the impairment of neurogenesis was reported to affect hippocampal-associated cognitive functions (56). Our findings on the functional effects of RNA editing of $Ca_V1.3$ channels on the hippocampal neurons provide insight to further investigate how a gain of function due to loss of $Ca_V1.3$ RNA editing may impact neuronal neurogenesis and differentiation.

Materials and Methods

Generation of Genetically Modified $Ca_V1.3^{\Delta ECS/\Delta ECS}$ Mice. The strategy to generate an ECS targeting construct is summarized in *SI Appendix*, Fig. S1*A*. The embryonic stem cells that had undergone homologous recombination were injected into SV129 mouse blastocysts. Male and high agouti-color coated F0 mice were selected to mate with C57BL/6 female mice to generate F1 pups. Genotyping was performed using PCR and Southern blot analysis. Details are found in *SI Appendix, Supplemental Experimental Procedures*.

Evaluation of IQ-Domain RNA Editing in $Ca_V1.3$ Channels. Total RNA was isolated from brain tissues using the TRIzol method (Invitrogen), and first-strand complementary DNA (cDNA) was synthesized with SuperScript II and oligo(dT)18 primers (Invitrogen). RNA was treated with DNase I (Invitrogen) before being subjected to reverse transcription. For tissues collected from mouse, rat, and *Macaca fascicularis*, all experimental procedures were approved by Institutional Animal Care and Use Committee (IACUC) at the National University of Singapore. For the postmortem brain samples from various animals from the Mandai Wildlife Group (MWG), all procedures were approved by IACUC at the MWG Research Panel. For humans, the Whole Brain Marathon-Ready cDNA library (Clontech, Takara) was used. PCR was performed with primers designed for different species (listed in *SI Appendix*, Table S1). Details are found in *SI Appendix, Supplemental Experimental Procedures*.

The level of RNA editing was calculated by measuring the heights of the peaks of A/G on the electropherograms obtained from DNA sequencing:

$$\text{The editing level } (\%) = \text{height (G)}/[\text{height (A)} + \text{height (G)}] * 100\%.$$

Immunoblotting. To validate the expression level of targeted proteins, brain tissues or hippocampal slices were dissected on ice and were snap-frozen immediately. The CA1 region was then isolated carefully under a dissection microscope at 4 °C. Details are found in *SI Appendix, Supplemental Experimental Procedures*.

Hippocampal Slice Preparation. $Ca_V1.3^{\Delta ECS}$ and WT mice maintained on a 12 h light/dark cycle were used in these studies. All experimental procedures were approved by IACUC at the National University of Singapore. For the whole-cell patch-clamp recordings, male mice (aged 5–7 wk) were anesthetized deeply with isoflurane (0.5 mL) before cervical dislocation. Mice were then decapitated; brains were removed quickly and placed in a dissection medium containing ice-cold sucrose–artificial cerebrospinal fluid (ACSF). Coronal slices (280–300 μm thickness) including the hippocampi were cut using a vibrating microtome (Leica 1200S). Slices were first incubated in a chamber containing ACSF for 30 to 45 min at 32 °C and then maintained at room temperature. Single slices were transferred to the recording chamber and superfused with ACSF bubbled with 95% O_2–5% CO_2. The composition of ACSF was as follows (in mM): 125 NaCl, 2.5 KCl, 1.25 Na_2HPO_4, 25 $NaHCO_3$, 25 glucose, 1 $MgSO_4$, and 2 $CaCl_2$ (300–310 mosmol/L, pH 7.4). For the sucrose–ACSF solution, NaCl was substituted by sucrose (230 mM) and the concentrations of $MgSO_4$ and $CaCl_2$ were modified to 5 mM and 0.5 mM, respectively, and an additional 3 mM myo-inositol, 2 mM Na-pyruvate, and 0.4 mM ascorbic acid (320–330 mosmol/L, pH 7.3).

Whole-Cell Patch-Clamp Electrophysiological Recordings. The soma of CA1 and CA3 pyramidal cells were visually identified using a Nikon Eclipse FN1 equipped with a 40× water immersion objective and a CoolSnap EZ camera. Brain slices were constantly perfused with the above-mentioned oxygenated ACSF at a flow rate of 1.5 to 2 mL/min at room temperature. Whole-cell patch-clamp electrophysiological recordings were conducted using an EPC-9 or EPC-10 USB amplifier controlled by Patchmaster (Heka Elektronik, Lambrecht, Germany). Patch pipettes of 3 to 5 MΩ were pulled from borosilicate glass capillaries using a vertical Narishige PC-10 puller (Japan). Whole-cell patch-clamp recordings were performed with CA1 and CA3 pyramidal neurons from both $Ca_V1.3^{ECS}$ and $Ca_V1.3^{\Delta ECS}$ mice. Details are found in *SI Appendix, Supplemental Experimental Procedures*.

Field Recording. Transverse hippocampal slices of 400 μm thickness were prepared from the right and left hippocampus using a manual tissue chopper (Stoelting, Wood Dale, IL) and transferred onto a nylon net placed in an interface chamber (Scientific Systems Design, Ontario, Canada) and incubated at 32 °C at an ACSF flow rate of 1 mL/min and carbogen consumption of 16 L/h. The entire process of animal dissection, hippocampal slice preparation, and placement of slices on the chamber was completed within approximately 5 min to ensure that hippocampal slices were in good condition for electrophysiology studies. The slices were incubated for at least 3 h before starting the experiments.

In all the field electrophysiology recordings, single-pathway experiments were performed. A single monopolar lacquer-coated stainless-steel electrode (5MΩ; AM Systems, Sequim) was positioned in the stratum radiatum of the CA1 region for stimulating a neuronal population, thus evoking field excitatory postsynaptic potentials (fEPSP) from Schaffer collateral/commissural-CA1 synapses (Fig. 1*A*). Details are found in *SI Appendix, Supplemental Experimental Procedures*.

Data Analysis. The peak current of Ca^{2+} and K^+ at different holding potentials was analyzed using Fit-master (HEKA Electronics). I-V curves of Ca^{2+} currents were fitted by

$$I = G_{max} * (V - E_{rev})/\{1 + \exp[(V - V_{1/2})/k]\},$$

where G_{max} is the maximum conductance of the cell, E_{rev} is the reversal potential, $V_{1/2}$ is the voltage for half-maximal activation, and k is the slope factor of Boltzmann function.

Action potential firing frequency, half-width, and threshold were measured by automatic detection and calculation using customized MATLAB scripts adapted from a published algorithm (57). Briefly, the action potential amplitude (baseline to action potential peak value) was measured and the time between the half-peak amplitude on the rising and falling phases was taken to be the action potential half-width. The spike threshold was defined as the time point when the membrane potential increasing slope was 5 mV/ms. The mEPSCs were analyzed using the Mini Analysis Program (Synaptosoft Inc), and AMPDAR/NMDAR ratios were analyzed using customized MATLAB scripts.

For field recordings, the fEPSP slope value, expressed as percentages of average baseline values per time point, was subjected to statistical analysis using GraphPad Prism (GraphPad, San Diego, CA). Nonparametric tests were selected because a normal distribution could not always be assumed with the sample size per series and analyses of prolonged recordings do not allow the use of parametric tests. Furthermore, the sample sizes did not always guarantee a Gaussian normal distribution of the data per series. The Wilcoxon signed rank test was used to compare fEPSP values within one group and the Mann–Whitney *U* test was used when data were compared between groups. $P < 0.05$ was considered as the cut-off for statistically significant difference, n represented the number of slices, and a minimum of five animals were used for each experiment.

Clearing of Hippocampal Slices. To label the CA1 pyramidal neurons for examining morphological changes, 10 mM Alexa Fluor 488 hydrazide (A10436; Thermo Fisher Scientific) was loaded into the neurons under a whole-cell patch-clamp configuration with an internal solution used for mEPSC recording. The neurons were held at −70 mV for 15 min for the dye to diffuse first into the soma and then into the dendrites. Next, slices with labeled CA1 neurons were fixed in 4% PFA for 30 min at room temperature, followed by three washes in PBS before treatment in 0.5% PBST overnight. The slices were then transferred in RapiClear 1.47 (SunJin Lab) for at least 3 h and mounted in fresh RapiClear 1.47. All mounted samples were kept at 4 °C before confocal imaging.

Confocal Imaging and Image Analysis. Images were taken with a laser scanning microscope (FV3000; Olympus) using an excitation wavelength of 488 nm and PlanApo (10×/0.40) and UPLSAPO (60×/1.35) objective lenses (Olympus). Dye-injected hippocampal pyramidal neurons were imaged using the multi-area time–lapse function comprising 4 × 3 tiles (each tile, 1024 × 1024 pixels), with the *z* axis range decided by manually adjusting the focal depth until no signal from the neuron could be observed.

Images were analyzed using a commercially available software, Filament Tracer (Imaris, Bitplane, Inc). Prior to neuron tracing, background fluorescent signals were removed using the mask function of Imaris. The neurons were traced using a semiautomated mode, Autopath, in the Imaris Filament Tracer. Traced neurons were then exported as images that were further used for Sholl analysis in ImageJ. Dendritic spines were semiautomatically traced single-blind in Imaris with auto-depth function on dendritic branches that were 100 to 200 μm from the soma. Dendritic spine numbers were subsequently obtained from the statistic tab in Imaris.

Morris Water Maze. Spatial reference memory and insistence on sameness were tested in a circular tank (diameter, 183 cm) filled with water and surrounded by uniform curtains and visual cues. The water was made opaque by adding a sufficient amount of tempera paint. Animal movements were tracked using a ceiling camera and Topscan tracking software. Mice were introduced into the pool at pseudorandomized drop locations outside of the target quadrant. During the "hidden platform learning task," an escape platform (15 cm) was placed in the middle of a designated target quadrant 1 cm below the water surface. Mice were trained to find the platform by four 60 s trials per day for 4 consecutive days. A trial ended either when a mouse rested on the hidden platform for 5 s or the end of the trial was reached. Mice who had failed to find the platform were then manually guided to it. On day 1, 30 min after completing 4 training trials, a short-term probe test was conducted with the escape platform removed. On day 5, a long-term probe test was conducted and a remote probe test was conducted on day 12. Latency to find the hidden platform was obtained during the training trials. An average latency of four trials was calculated for the learning curve. Time spent in quadrants was tracked during probe tests.

Data Availability. All study data are included in the article and/or *SI Appendix*.

ACKNOWLEDGMENTS. We thank Shun Qiang Lo and Qiang Yuan for help with MATLAB scripts and Thomas Behnisch (Fudan University) for suggestions on evoke EPSC and PPR experiments. We thank Thomas Sudhof for the gift of the p-Syn-1 and Syn-1 antibodies. We thank the Neuroscience Phenotyping Core for guidance and support for the behavioral tests, the Advance Imaging Laboratory for support for confocal imaging, and the Conservation, Research and Veterinary (CRV) and Animal Care teams of Mandai Wildlife Group for the postmortem brain samples from various animals. The generation of $Ca_V1.3^{\Delta ECS}$ mice in the paper was developed from Jing Zhai's thesis.

Author affiliations: [a]Department of Physiology, National University of Singapore, Singapore 117593; [b]Lee Kong Chian School of Medicine, Nanyang Technological University, Singapore 308232; [c]Animal Gene Editing Laboratory, Biological Resource Center, Agency for Science, Technology and Research, Singapore 117684; [d]Healthy Longevity Translational Research Programme, Yong Loo Lin School of Medicine, National University of Singapore, Singapore, 117456; and [e]Electrophysiology Core Facility, Yong Loo Lin School of Medicine, National University of Singapore, Singapore 117593

1. G. Xu, J. Zhang, Human coding RNA editing is generally nonadaptive. *Proc. Natl. Acad. Sci. U.S.A.* **111**, 3769–3774 (2014).
2. Z. Peng *et al.*, Comprehensive analysis of RNA-seq data reveals extensive RNA editing in a human transcriptome. *Nat. Biotechnol.* **30**, 253–260 (2012).
3. R. T. O'Neil, X. Wang, M. V. Morabito, R. B. Emeson, Comparative analysis of A-to-I editing in human and non-human primate brains reveals conserved patterns and context-dependent regulation of RNA editing. *Mol. Brain* **10**, 11 (2017).
4. N. Liscovitch-Brauer *et al.*, Trade-off between transcriptome plasticity and genome evolution in cephalopods. *Cell* **169**, 191–202.e11 (2017).
5. S. C. Garrett, J. J. Rosenthal, A role for A-to-I RNA editing in temperature adaptation. *Physiology (Bethesda)* **27**, 362–369 (2012).
6. H. E. Krestel *et al.*, A genetic switch for epilepsy in adult mice. *J. Neurosci.* **24**, 10568–10578 (2004).
7. Y. Kawahara *et al.*, Dysregulated editing of serotonin 2C receptor mRNAs results in energy dissipation and loss of fat mass. *J. Neurosci.* **28**, 12834–12844 (2008).
8. C. B. Martin *et al.*, RNA splicing and editing modulation of 5-HT(2C) receptor function: Relevance to anxiety and aggression in VGV mice. *Mol. Psychiatry* **18**, 656–665 (2013).
9. H. Huang *et al.*, RNA editing of the IQ domain in Ca(v)1.3 channels modulates their Ca^{2+}-dependent inactivation. *Neuron* **73**, 304–316 (2012).
10. H. Bazzazi, M. Ben Johny, P. J. Adams, T. W. Soong, D. T. Yue, Continuously tunable Ca(2+) regulation of RNA-edited CaV1.3 channels. *Cell Rep.* **5**, 367–377 (2013).
11. P. J. Adams, M. Ben-Johny, I. E. Dick, T. Inoue, D. T. Yue, Apocalmodulin itself promotes ion channel opening and Ca(2+) regulation. *Cell* **159**, 608–622 (2014).
12. T. Bhalla, J. J. Rosenthal, M. Holmgren, R. Reenan, Control of human potassium channel inactivation by editing of a small mRNA hairpin. *Nat. Struct. Mol. Biol.* **11**, 950–956 (2004).
13. C. Daniel, H. Wahlstedt, J. Ohlson, P. Björk, M. Ohman, Adenosine-to-inosine RNA editing affects trafficking of the gamma-aminobutyric acid type A (GABA(A)) receptor. *J. Biol. Chem.* **286**, 2031–2040 (2011).
14. H. Huang *et al.*, Tissue-selective restriction of RNA editing of CaV1.3 by splicing factor SRSF9. *Nucleic Acids Res.* **46**, 7323–7338 (2018).
15. J. C. Magee, R. B. Avery, B. R. Christie, D. Johnston, Dihydropyridine-sensitive, voltage-gated Ca2+ channels contribute to the resting intracellular Ca2+ concentration of hippocampal CA1 pyramidal neurons. *J. Neurophysiol.* **76**, 3460–3470 (1996).
16. R. B. Avery, D. Johnston, Multiple channel types contribute to the low-voltage-activated calcium current in hippocampal CA3 pyramidal neurons. *J. Neurosci.* **16**, 5567–5582 (1996).
17. W. Xu, D. Lipscombe, Neuronal Ca(V)1.3alpha(1) L-type channels activate at relatively hyperpolarized membrane potentials and are incompletely inhibited by dihydropyridines. *J. Neurosci.* **21**, 5944–5951 (2001).
18. B. Li *et al.*, Neuronal inactivity co-opts LTP machinery to drive potassium channel splicing and homeostatic spike widening. *Cell* **181**, 1547–1565.e15 (2020).
19. O. Vivas, C. M. Moreno, L. F. Santana, B. Hille, Proximal clustering between BK and $Ca_V1.3$ channels promotes functional coupling and BK channel activation at low voltage. *eLife* **6**, 6 (2017).
20. T. Goodman *et al.*, Young hippocampal neurons are critical for recent and remote spatial memory in adult mice. *Neuroscience* **171**, 769–778 (2010).
21. B. C. McKinney, G. G. Murphy, The L-type voltage-gated calcium channel Cav1.3 mediates consolidation, but not extinction, of contextually conditioned fear in mice. *Learn. Mem.* **13**, 584–589 (2006).
22. B. C. McKinney, W. Sze, J. A. White, G. G. Murphy, L-type voltage-gated calcium channels in conditioned fear: A genetic and pharmacological analysis. *Learn. Mem.* **15**, 326–334 (2008).
23. B. G. Hiester *et al.*, L-type voltage-gated Ca^{2+} channels regulate synaptic-activity-triggered recycling endosome fusion in neuronal dendrites. *Cell Rep.* **21**, 2134–2146 (2017).
24. Y. Kawamura *et al.*, The CB1 cannabinoid receptor is the major cannabinoid receptor at excitatory presynaptic sites in the hippocampus and cerebellum. *J. Neurosci.* **26**, 2991–3001 (2006).
25. A. Fletcher-Jones *et al.*, Protein interactors and trafficking pathways that regulate the cannabinoid type 1 receptor (CB1R). *Front. Mol. Neurosci.* **13**, 108 (2020).
26. G. W. Zamponi, K. P. Currie, Regulation of Ca(V)2 calcium channels by G protein coupled receptors. *Biochim. Biophys. Acta* **1828**, 1629–1643 (2013).
27. K. Mackie, B. Hille, Cannabinoids inhibit N-type calcium channels in neuroblastoma-glioma cells. *Proc. Natl. Acad. Sci. U.S.A.* **89**, 3825–3829 (1992).
28. M. Liu, B. Yu, O. Nakanishi, T. Wieland, M. Simon, The Ca2+-dependent binding of calmodulin to an N-terminal motif of the heterotrimeric G protein beta subunit. *J. Biol. Chem.* **272**, 18801–18807 (1997).
29. K. P. Currie, G protein modulation of CaV2 voltage-gated calcium channels. *Channels (Austin)* **4**, 497–509 (2010).
30. T. J. Bell, C. Thaler, A. J. Castiglioni, T. D. Helton, D. Lipscombe, Cell-specific alternative splicing increases calcium channel current density in the pain pathway. *Neuron* **41**, 127–138 (2004).
31. D. G. Wheeler *et al.*, Ca(V)1 and Ca(V)2 channels engage distinct modes of Ca(2+) signaling to control CREB-dependent gene expression. *Cell* **149**, 1112–1124 (2012).
32. K. Shen, T. Meyer, Dynamic control of CaMKII translocation and localization in hippocampal neurons by NMDA receptor stimulation. *Science* **284**, 162–166 (1999).
33. K. Okamoto, R. Narayanan, S. H. Lee, K. Murata, Y. Hayashi, The role of CaMKII as an F-actin-bundling protein crucial for maintenance of dendritic spine structure. *Proc. Natl. Acad. Sci. U.S.A.* **104**, 6418–6423 (2007).
34. C. Patzke *et al.*, Neuromodulator signaling bidirectionally controls vesicle numbers in human synapses. *Cell* **179**, 498–513.e22 (2019).
35. J. G. McLarnon, Inactivation of a high conductance calcium dependent potassium current in rat hippocampal neurons. *Neurosci. Lett.* **193**, 5–8 (1995).
36. L. R. Shao, R. Halvorsrud, L. Borg-Graham, J. F. Storm, The role of BK-type Ca2+-dependent K+ channels in spike broadening during repetitive firing in rat hippocampal pyramidal cells. *J. Physiol.* **521**, 135–146 (1999).
37. B. Wang, D. B. Jaffe, R. Brenner, Current understanding of iberiotoxin-resistant BK channels in the nervous system. *Front. Physiol.* **5**, 382 (2014).
38. P. Y. Deng *et al.*, FMRP regulates neurotransmitter release and synaptic information transmission by modulating action potential duration via BK channels. *Neuron* **77**, 696–711 (2013).
39. J. R. M. Harvey, A. E. Plante, A. L. Meredith, Ion channels controlling circadian rhythms in suprachiasmatic nucleus excitability. *Physiol. Rev.* **100**, 1415–1454 (2020).
40. E. B. Han, C. F. Stevens, Development regulates a switch between post- and presynaptic strengthening in response to activity deprivation. *Proc. Natl. Acad. Sci. U.S.A.* **106**, 10817–10822 (2009).
41. J. Noel *et al.*, Surface expression of AMPA receptors in hippocampal neurons is regulated by an NSF-dependent mechanism. *Neuron* **23**, 365–376 (1999).
42. Z. Ye, R. H. Cudmore, D. J. Linden, Estrogen-dependent functional spine dynamics in neocortical pyramidal neurons of the mouse. *J. Neurosci.* **39**, 4874–4888 (2019).
43. C. S. Chan *et al.*, "Rejuvenation" protects neurons in mouse models of Parkinson's disease. *Nature* **447**, 1081–1086 (2007).
44. E. Ilijic, J. N. Guzman, D. J. Surmeier, The L-type channel antagonist isradipine is neuroprotective in a mouse model of Parkinson's disease. *Neurobiol. Dis.* **43**, 364–371 (2011).
45. A. Kupsch *et al.*, 1-Methyl-4-phenyl-1,2,3,6-tetrahydropyridine-induced neurotoxicity in non-human primates is antagonized by pretreatment with nimodipine at the nigral, but not at the striatal level. *Brain Res.* **741**, 185–196 (1996).
46. A. Hetzenauer, M. J. Sinnegger-Brauns, J. Striessnig, N. Singewald, Brain activation pattern induced by stimulation of L-type Ca2+-channels: Contribution of Ca(V)1.3 and Ca(V)1.2 isoforms. *Neuroscience* **139**, 1005–1015 (2006).
47. P. Busquet *et al.*, CaV1.3 L-type Ca2+ channels modulate depression-like behaviour in mice independent of deaf phenotype. *Int. J. Neuropsychopharmacol.* **13**, 499–513 (2010).
48. I. Iossifov *et al.*, De novo gene disruptions in children on the autistic spectrum. *Neuron* **74**, 285–299 (2012).
49. B. J. O'Roak *et al.*, Sporadic autism exomes reveal a highly interconnected protein network of de novo mutations. *Nature* **485**, 246–250 (2012).
50. A. Pinggera *et al.*, CACNA1D de novo mutations in autism spectrum disorders activate Cav1.3 L-type calcium channels. *Biol. Psychiatry* **77**, 816–822 (2015).
51. U. I. Scholl *et al.*, Somatic and germline CACNA1D calcium channel mutations in aldosterone-producing adenomas and primary aldosteronism. *Nat. Genet.* **45**, 1050–1054 (2013).
52. K. Khermesh *et al.*, Reduced levels of protein recoding by A-to-I RNA editing in Alzheimer's disease. *RNA* **22**, 290–302 (2016).
53. S. Wu, M. Yang, P. Kim, X. Zhou, ADeditome provides the genomic landscape of A-to-I RNA editing in Alzheimer's disease. *Brief. Bioinform.* **22**, bbaa384 (2021).
54. Y. Mizuno *et al.*, MUTYH actively contributes to microglial activation and impaired neurogenesis in the pathogenesis of Alzheimer's disease. *Oxid. Med. Cell. Longev.* **2021**, 8635088 (2021).
55. S. Morabito, E. Miyoshi, N. Michael, V. Swarup, Integrative genomics approach identifies conserved transcriptomic networks in Alzheimer's disease. *Hum. Mol. Genet.* **29**, 2899–2919 (2020).
56. J. Marschallinger *et al.*, The L-type calcium channel Cav1.3 is required for proper hippocampal neurogenesis and cognitive functions. *Cell Calcium* **58**, 606–616 (2015).
57. A. X. Sun *et al.*, Potassium channel dysfunction in human neuronal models of Angelman syndrome. *Science* **366**, 1486–1492 (2019).